Title
Characterization of Seismic Levee Fragility Using Field Performance Data

Journal
Earthquake Spectra, 32(1)

ISSN
8755-2930

Authors
Kwak, Dong Youp
Stewart, Jonathan P
Brandenberg, Scott J
et al.

Publication Date
2016-02-01

DOI
10.1193/030414eqs035m

Peer reviewed

Characterization of Seismic Levee Fragility using Field Performance Data

Dong Youp Kwak,[a] S.M.EERI, Jonathan P. Stewart,[a] M.EERI, Scott J. Brandenberg,[a] M.EERI, and Atsushi Mikami[b]

We characterize the seismic fragility of levees along the Shinano River system in Japan using field performance data from two **M** 6.6 shallow crustal earthquakes. Levee damage is quantified based on crack depth, crack width, and crest subsidence for 3318 levee segments each 50 m long. Variables considered for possible correlation to damage include peak ground velocity (*PGV*), geomorphology, groundwater elevation, and levee geometry. Seismic levee fragility is expressed as the probability of exceeding a damage level conditioned on *PGV* alone and *PGV* in combination with other predictive variables. The probability of damage (at any level) monotonically increases from effectively zero for *PGV* < 14 cm/s to approximately 0.5 for *PGV* ≈ 80 cm/s. Of the additional parameters considered, groundwater elevation relative to levee base most significantly affects fragility functions, increasing and decreasing failure probabilities (relative to the *PGV*-only function) for shallow and deep groundwater conditions, respectively.

INTRODUCTION

A levee is a natural or artificial embankment that provides flood protection adjacent to rivers or coastal areas. Most often flood control levees do not routinely retain water, serving that function only during flood events that are unlikely to coincide with a major earthquake. The objective of this research is to empirically characterize the seismic fragility of flood control levees from experience in a region where levee systems have been strongly shaken by multiple shallow crustal earthquakes.

Because levees are often constructed on soft soils, seismic hazards are generally driven by ground failure involving weak and potentially liquefiable soils in the foundations and in the levees themselves. Recently developed levee design standards consider seismic demands

[a] Civil & Env. Eng. Dept., UCLA, Los Angeles, CA
[b] Civil & Env. Eng. Dept., Univ. of Tokushima, Japan

(USACE, 2011; Sugita and Tamura, 2008; MLIT, 2012), but the principal problem remains the substantial levee networks already in place that were not properly engineered at the time of their original construction.

Several prior studies have examined individual case histories of seismic levee failures, typically from liquefaction of embankment or foundation materials (Sasaki, 2009; Miller and Roycroft, 2004). The present work is fundamentally different in scope in two respects: (1) instead of looking at individual deformed sections, we systematically examine levee performance at a regular spacing interval along a river system, including segments with and without ground deformations; (2) we analyze damage relative to simple parameters representing seismic demand and levee/ground conditions in lieu of detailed, site-specific geotechnical analysis.

Our results are expressed in terms of fragility functions that give the probability of damage as a function of ground motion intensity and other relevant factors. These are not the first fragility functions that have been developed for levees. Salah-Mars et al. (2008) estimated fragility for levees in the California Bay Delta region based on numerical analyses of seismic levee deformation potential combined with judgment-based relations for breach probability conditional on crest settlement. Rosidi (2007) evaluated levee fragility in a broadly similar manner for generic levee sections (not specific to a location). Moreover, procedures to estimate levee fragility for non-seismic hazards have been established from analytical simulations by Apel et al. (2004) and Vorogushyn et al. (2009) (instabilities from overtopping and piping, respectively, from river water rise) and from a combination of analysis and observation by Foster et al. (2009) (overtopping and seepage). Our study is distinct from prior work in that seismic fragilities are estimated directly from analysis of field performance data, without an underlying numerical model of soil response. Our results provide probabilities of various damage states, not of a binary failure or non-failure condition. As such, our work is similar in objective (if not in approach) to the first step of the fragility development process defined by Salah-Mars et al. (2008) and Rosidi (2007) (i.e., computation of deformation given ground motion level). Our estimates of fragility are useful for preliminary seismic risk assessments of this critical infrastructure for regions having similar seismologic, hydrologic, and geologic conditions to those in the study region, particularly when detailed geotechnical data is not available.

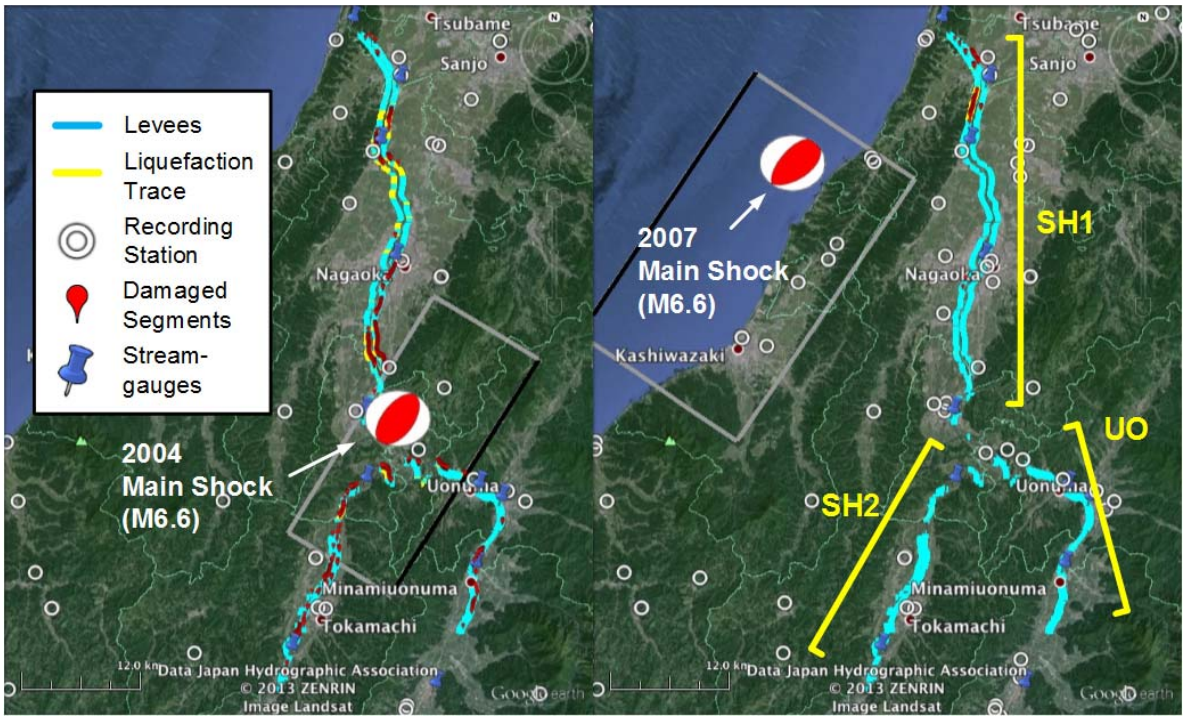

Figure 1. Levees along the Shinano River system (SH1, SH2, and UO) on Google Earth map. Locations of levee damage, liquefaction trace, epicenters (beach balls) and finite fault planes (black line at top). Locations of recording stations and stream gauges. Finite fault solutions from Asano and Iwata (2009) and Miyake et al. (2010).

Figure 1 shows the study region including levees along the Shinano River system and finite fault solutions for the two considered reverse-slip events (2004 **M** 6.6 Niigata-ken Chuetsu and 2007 **M** 6.6 Niigata-ken Chuetsu-oki earthquakes). This data set was selected because:

i. Levee performance was well documented by staff of the Shinano River Work Office (SWO) under MLIT and the Niigata Prefectural Office agencies (NPO) in Japan (whose staff manually inspected the full length of the levees in the effected regions),

ii. The level of ground shaking varied across the levee system such that some areas were strongly shaken on the surface projection of the fault ruptures (maximum recorded *PGA* ≈ 1.6g) and experienced damage, whereas other areas experienced more modest shaking and little damage (thereby bracketing a range of responses),

iii. Significant geotechnical data have been compiled for the region as part of engineering investigations, and

iv. The earthquake magnitudes were generally comparable with design-basis earthquakes in other regions where the results are needed for application, including much of California's Central Valley region.

Subsequent sections describe the work undertaken to evaluate levee fragility, including the assignment of damage categories, analysis of ground motion intensity measures, analysis of ground water levels, and assignment of geomorphic categories and levee shape parameters. We then describe the function adopted for fragility curves, the regression process, and our interpretation of the results. There are several topics we recognize as significant that are not covered here, including development of fragility relations in which the demand is represented by a deformation index from geotechnical analysis (e.g., Newmark displacement, lateral displacement index) and the analysis of spatial correlations in levee performance. The later issue is particularly important to the application of the present results to a distributed system of levees as would be encountered in practical applications. These technical issues will be addressed in later publications.

LEVEE DAMAGE DOCUMENTATION

As shown in Figure 1, the Shinano River system in Japan has three components -- Shinano River mid- and downstream (SH1), Shinano River upstream (SH2), and the tributary Uono River (UO). The 2004 earthquake fault plane was located beneath the river system and produced broadly distributed damage. Many segments experienced strong shaking (up to 1.6g *PGA*). The 2007 earthquake fault plane was located off-shore and produced modest shaking intensity in the study region (0.1~0.4g *PGA*). Damage was concentrated in downstream portions of the levee system. Figure 1 also shows locations of surface manifestation of liquefaction, some (but not all) of which are co-located with areas of levee damage.

The locations and severity of damage are based on post-earthquake damage reports by the Shinano River Work Office (SWO, 2007, 2008) and OYO (2008), which measured at regular intervals crack depth and width, vertical slip across cracks, and relative settlement between damaged and undamaged levee sections. The SWO reports also provide a photographic record of the levee performance at regular intervals. Segments without measured damage quantities did not suffer damage beyond a visually apparent level, and are confirmed cases of no damage rather than levee segments that were not inspected. Figure 2 shows examples of various damage states.

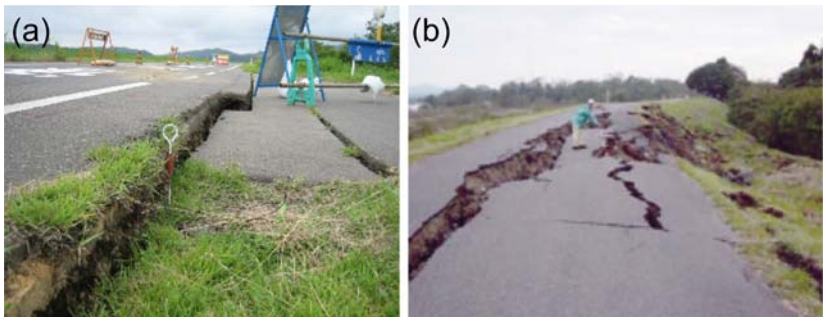

Figure 2. Example of damage states on levee. (a) Damage level 2: crack ~ 7 km inland from ocean at the Shinano River during 2007 earthquake (from OYO, 2008) and (b) damage level 4: lateral spreading ~ 40 km inland from ocean during 2004 earthquake (from SWO, 2008).

We classify damage severity in five levels as shown in Table 1 for 50 m (in length) levee segments throughout the Shinano River system (3318 segments up to 80 km from river mouth). To place the subsidence numbers in perspective, average levee heights range from 5.7 to 4.5 m in downstream and upstream areas, respectively, so the subsidence associated with damage level 4 (i.e., > 100 cm) corresponds to at least 20% of the levee height. When the available damage metrics produce different damage classifications for a given levee segment, we select the most severe classification. Of the 3318 segments, damage levels of one or greater were found for 652 segments in the 2004 event and 78 segments in the 2007 event (damage rates of 19.7% and 2.4%, respectively).

Table 1. Damage levels assigned to levee segments

Damage Level	Crack depth (cm)	Crack width (cm)	Subsidence (cm)	Description
0	0	0	0	No damage reported
1	0~100	0~10	0~10	Slight damage, small cracks
2	100~200	10~50	10~30	Moderate damage, cracks or small lateral spreading
3	200~300	50~100	30~100	Severe damage, lateral spreading
4	> 300	> 100	> 100	Levee collapse

Figure 3 shows rates of surface manifestation of liquefaction conditional on damage level. Levee segments with no or minor damage levels (DL = 0 and 1) have low rates of liquefaction manifestation, whereas levees with moderate to severe damage levels (DL > 1) have surface manifestation rates of 50-80%. This indicates that damaged levee segments were often, but not always, accompanied by the surface manifestation of liquefaction.

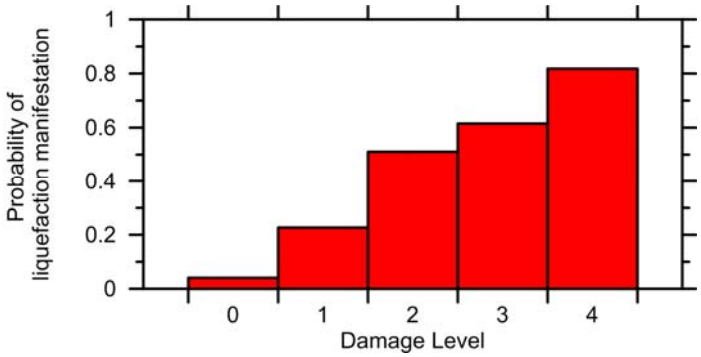

Figure 3. Probability of surface manifestation of liquefaction for each damage level.

GROUND MOTION DISTRIBUTION

There are a substantial number of ground motion stations in the study region, but with few exceptions, accelerographs are not located sufficiently near levees to evaluate directly ground motion intensities at levee sections. Moreover, direct Kriging (i.e., simple spatial interpolation) of intensity measures (e.g., *PGA* or *PGV*) is problematic, because the site conditions at recording stations tend to be systematically firmer than those at levee sites, thus the locations of the measurements and the application sites have different levels of site response.

Accordingly, to estimate spatially distributed ground motions, we developed the following procedure:

1) Estimate V_{S30} (time-averaged shear wave velocity in upper 30 m of site) for the foundation conditions beneath levees and recording sites using velocity measurements where available, and otherwise using region-specific V_S-SPT correlations described in Stewart et al. (2013).

2) For earthquake *i*, compute within-event residuals as the difference between intensity measures from recording *j* and the mean from a selected ground motion prediction equation (GMPE) computed for the magnitude, distance, and site conditions present at site *j* for event *i*. This residual is computed as follows:

$$R_{i,j} = \ln\left(IM_{i,j}^{rec}\right) - \left(\mu_{i,j} + \eta_i\right), \tag{2}$$

where $IM_{i,j}^{rec}$ denotes the intensity measure from recording *j*, $\mu_{i,j}$ is the GMPE mean in natural log units, and η_i is the event term (effectively the mean residual for event *i* for well-recorded events). We use the Boore et al. (2014) (BEA) GMPE.

3) Map the spatial variation of residuals R_i using the simple Kriging method (no distance dependence). Details on the Kriging method used, including the applicable semi-variograms, are given in Kwak et al. (2012).

4) Calculate ground motion *IM*s for sites of interest as:

$$\ln\left(IM_{i,n}^{K}\right) = R_{i,n}^{K} + \mu_{i,n} + \eta_i, \tag{2}$$

where $R^{K}_{i,n}$ represents the mapped residual from (3), and index n refers to sites for which ground motions are to be estimated.

Relative to prior work (Yamazaki et al., 2000; Sawada et al., 2008), this procedure is different because it includes nonlinear site amplification factors, which is important due to the strength of the shaking and the softer site conditions beneath the levees compared with the recording stations.

Figure 4 shows within-event *PGV* residual contour maps produced in Step 3. The 2004 earthquake produces a patchwork of residuals, which are mostly positive in the near-fault region. For the 2007 earthquake, residuals are generally positive south of the hypocenter and negative to the north.

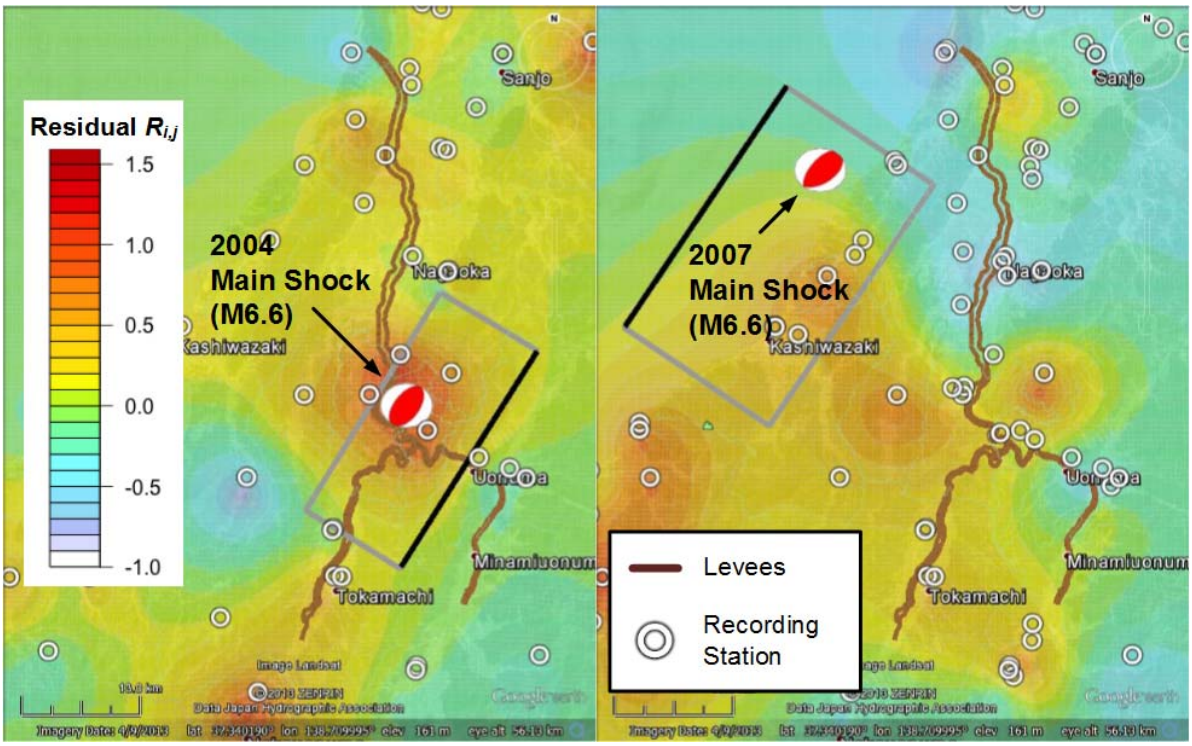

Figure 4. Contour maps of within-event *PGV* residuals from the Boore et al. (2014) GMPE for 2004 and 2007 earthquakes.

Figure 5 shows *PGV* profiles along the Shinano River levees produced by the proposed procedure and from relatively simple direct Kriging of ground motion data. The proposed procedure produces larger ground motion estimates (than those from direct Kriging) for levees near rock sites with moderate ground shaking (e.g., ~18 km from river mouth) and slightly smaller ground motions at most locations beyond 30 km from the river mouth. The larger ground motions near rock accelerograph sites result from relatively strong site responses at the levee sites, which amplify smaller estimated levee motions. In the regions beyond 30 km (from river mouth), typically the accelerographs and levee sites are both on soil, but small differences in the V_{S30} values (between accelerographs and levee sites) and the use of a nonlinear site term in the proposed procedure, produce the observed ground motion reductions.

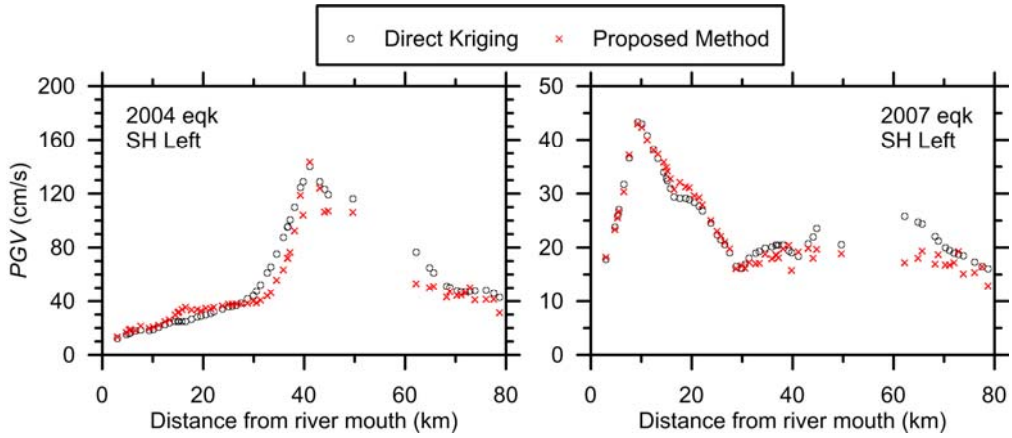

Figure 5. *PGV*s interpolated from seismic stations using direct Kriging and those estimated by proposed method using residuals analysis from a GMPE.

GROUNDWATER ELEVATION

We describe procedures for estimating groundwater elevation on the earthquake dates. Groundwater levels were measured in geotechnical borings, but those water levels may not match those during earthquakes due to variations in the river water level over time and local agricultural practices. We estimate groundwater level on the earthquake date based on (*i*) measurements of levee groundwater elevation (*LGWE*) at the time of a geotechnical boring, (*ii*) measurements of river water elevation (*RWE*) from stream gauge stations on the borehole date, and (*iii*) *RWE* on the earthquake date.

Our approach is to use available borehole data to evaluate the differential between *LGWE* and *RWE* at the time of subsurface exploration. This differential is then added to the *RWE* at the time of the earthquake to estimate *LGWE* on the earthquake date. A key assumption is

that the *RWE* is directly related to *LGWE* since levees are adjacent to the river, but adjustments are made for levees with land-side irrigation. We describe below how *RWE* and *LGWE* were obtained and analysis of the *LGWE*-*RWE* differential.

GROUNDWATER ELEVATION IN BOREHOLES

Starting before the 2004 earthquake, borings have been drilled by vendors contracted with SWO (references given in Stewart et al., 2013) along the Shinano River levees, up to 80 km from the river mouth, for the purpose of seepage and slope stability analyses. As shown in Figure 6, a given levee section typically has three borings − near the crest, river-side, and land-side slope or berm. Groundwater levels measured in borings are sensitive to the drilling method and in some cases were affected by in-situ permeability tests in which the water level in the boring was artificially adjusted to monitor seepage rate. Auger-drilled boreholes typically have water levels that rise with time towards the water table elevation. Rotary wash boreholes typically have water levels that drop with time towards the water table due to the use of drilling fluid.

We selected a representative water table elevation from borehole measurements in the following order of preference:

1. Water levels are taken from boreholes that are advanced without rotary wash drilling, without in-situ permeability tests, and located at levee crests.
2. Stabilized water elevations following in-situ permeability tests, irrespective of the drilling method.
3. When the method of drilling is unknown, select the last (in time) water elevation among the available measurements within the borehole at the levee crest.

The objective of this prioritization is to obtain a stable *LGWE* on the borehole date (or shortly thereafter), which may include perched ground water.

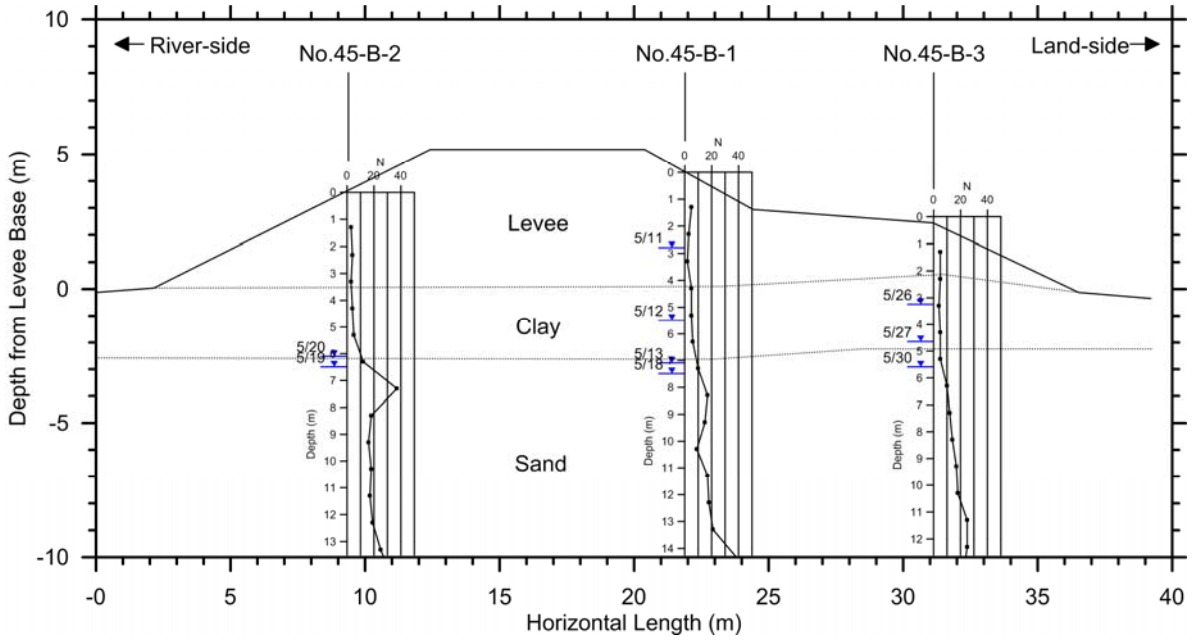

Figure 6. Example of cross sections through levee showing levee base and levee ground water elevations from boreholes on various dates (from OYO, 2008).

The total number of levee sections (similar to Figure 6) along the Shinano River system is 157, providing an average spacing of 1.0 km. Our analysis considers a far greater number of sections (3318) spaced 50 m apart. For sections without boreholes, *LGWE*s were linearly interpolated between those sections for which borehole data is available.

RIVER WATER ELEVATION

*RWE*s are measured from stream gauge stations hourly and daily; we sample the daily database on the earthquake date and the date of subsurface exploration. As shown in Figure 1, there are eleven stations along the study region, which is too sparse spatially (average distance between adjacent stations is 13 km) to provide accurate *RWE*s for each 50 m levee segment. For this reason, we also utilize *RWE* data from relatively detailed surveys performed after a flood (Oct 21 2004) and for maintenance purposes during a non-flood period having small *RWE* fluctuation (Oct 2009 ~ Feb 2010). These detailed surveys are used to improve our knowledge of the variation of *RWE* between stream gauges.

The relatively detailed surveys provide *RWE* profiles for portions of the levee system at a particular time; the data are not complete for the full 80 km of river length at any particular time, although data for the full river length are available for different times. The lengths of river for which the data at a given time apply are approximately 0.8 to 1.0 km (non-flood) and 10-30 km (flood). Given these complexities, the detailed survey data are best interpreted

relative to coincident stream gauge measurements that are linearly interpolated between stream gauges. This approach is effective because the stream gauge data is available at regular time intervals and can be matched to the times of detailed *RWE* measurements. Residual elevations (*R*) at location *x* and time *t* are computed as follows:

$$R(x,t) = RWE_{data}(x,t) - RWE_{sg-li}(x_i, x_{i+1}, x, t) \tag{3}$$

where x_i and x_{i+1} indicate locations of the stream gauges immediately down- and upstream of *x*, $RWE_{data}(x,t)$ indicates a measured elevation from detailed surveys, and $RWE_{sg\text{-}li}(x_i,x_{i+1},x,t)$ indicates the linearly interpolated *RWE* at location *x* and time *t* from the nearest stream gauges.

Residuals are computed for both flood and non-flood conditions. Each set is smoothed using a running Hann window (Oppenheim and Schafer, 2010) of width 2.0 km. The smoothed residuals depend only on location and are denoted $\overline{R}(x,set)$, where '*set*' refers to the data set being evaluated (*fl* for flood or *nfl* for non-flood). Using these smoothed residuals, high-resolution *RWE* profiles can be evaluated through simple re-arrangement of Eqn. (3):

$$RWE(x,t,set) = RWE_{sg-li}(x_i, x_{i+1}, x, t) + \overline{R}(x,set) \tag{4}$$

Having established the above procedure to compute detailed *RWE* profiles, the next issue concerns applying these procedures to specific points in time; in particular dates of subsurface investigation along levees and the two earthquake dates. In general, a given date of interest corresponds to conditions intermediate between 'flood' and 'non-flood', so a weighted average value of $\overline{R}$ is computed for application in Eqn. (4):

$$\overline{R}(x,t) = w_{fl}(x,t)\,\overline{R}(x,fl) + w_{nfl}(x,t)\,\overline{R}(x,nfl) \tag{5}$$

where w_{fl} and w_{nfl} are location- and time-specific weights that reflect the probability of having *RWE* at location *x* and time *t* corresponding to *fl* and *nfl* conditions, respectively. Those weights are computed from stream gauge *RWE*s upstream and downstream of *x* at time *t* (with greater emphasis on the most proximate gauges; equations given in Stewart et al. 2013). Weights evaluated using this process for borehole exploration dates emphasize the *nfl* condition because borings were generally drilled in non-flood season ($w_{nfl} \approx 1.0$; $w_{fl} \approx 0.0$). Weights for the earthquake dates were approximately $w_{nfl} \approx 0.61$ and $w_{fl} \approx 0.39$ (2004 event) and $w_{nfl} \approx 0.77$ and $w_{fl} \approx 0.23$ (2007 event).

Figure 7a shows *RWE*s during the flood event (Oct 21, 2004) and a representative date for the non-flood survey (Dec 1, 2009) along with linear interpolations between stream gauges. Those plots illustrate the poor fit of the linear interpolation function and the different shapes of the between-stream gauge *RWE* profiles for the *fl* and *nfl* conditions (particularly in the upstream region, > 60 km in SH2, and in the downstream region, < 10 km in SH1). These differences are what motivated the development of the interpolation scheme. A noteworthy feature of the *RWE* profiles occurs at x = 9.3 km, where the *nfl RWE*s abruptly drop 5 m but the *fl RWE* profiles are relatively flat. This difference occurs because of a weir at 9.3 km that retains a small reservoir under non-flood conditions and which overtops in floods.

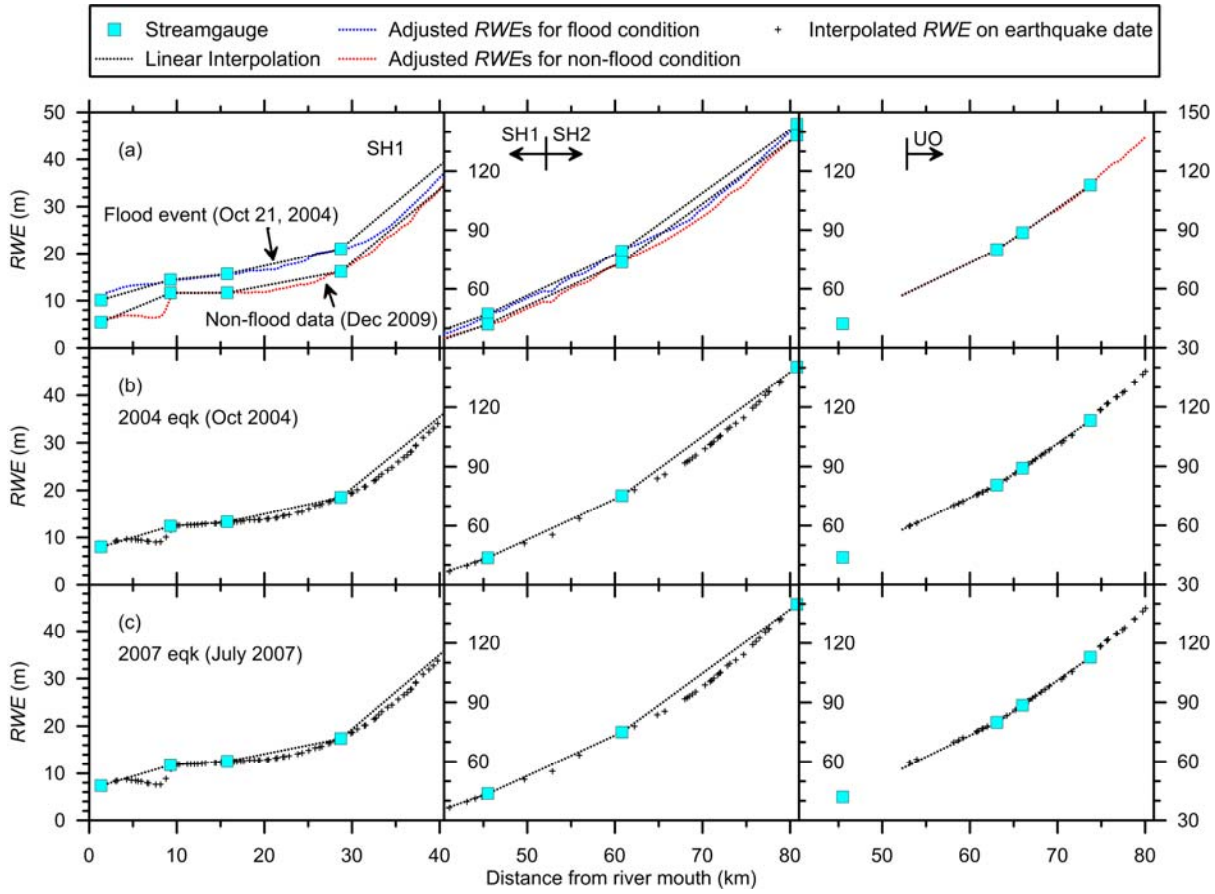

Figure 7. *RWE* profiles for (a) dates of detailed surveys for flood and non-flood conditions, (b) the 2004 earthquake, and (c) the 2007 earthquake dates. Linear interpolations between stream gauges are also shown.

Figures 7b and 7c show *RWE* profiles for the 2004 and 2007 earthquake dates as given by the above procedure with linear interpolation shown for reference purposes. Special accommodations were needed for the Uono River (UO) because it was not surveyed during the Oct 21 2004 flood event, although non-flood surveys are available. Thus, we use w_{nfl} =

1.0 in Eqn. (5) and the same spatial interpolation scheme described above for the Shinano River.

CORRELATION BETWEEN GROUNDWATER ELEVATION AND RIVER ELEVATION

We hypothesize that the difference between the ground water elevation beneath the levee (*LGWE*) and the river water elevation (*RWE*) might vary seasonally due to local agricultural practices on the land-side of the levees, thereby requiring a time-dependent adjustment. In this section, we examine profiles of this differential elevation over the river length and test its stability relative to periods of time when agriculture-related irrigation is or is not occurring.

Figure 8 shows *LGWE-RWE* differentials from all observed *LGWE*s in boreholes and from *LGWE*s screened as described above (i.e., data points meeting at least one of the three criteria). We plot the data separately for the growing and non-growing seasons. During the growing season (approximately June-September; FAO, 2004), there can be significant land-side irrigation for rice and other crops. As shown in Figure 8, in the mid- and downstream areas of the Shinano River (SH1) (river distance 15 ~ 25 km), the *LGWE-RWE* differential during the growing season is modestly greater than during the non-growing season for left-side levees, whereas both are similar for right-side levees. The differences between the two sides of the river can be explained based on the configuration of irrigation canals and other features (details in Stewart et al., 2013). In upstream areas (SH2 and UO; river distance > 50 km), borings were mostly performed during the non-growing season so differentials cannot be compared.

Based on the above, we conclude that during periods of heavy irrigation, the *LGWE* is controlled by irrigation and less influenced by *RWE* over the 15 ~ 25 km interval on left side levees, but elsewhere there is no tangible irrigation effects. Figure 8 shows the *LGWE-RWE* profiles adopted for subsequent analysis.

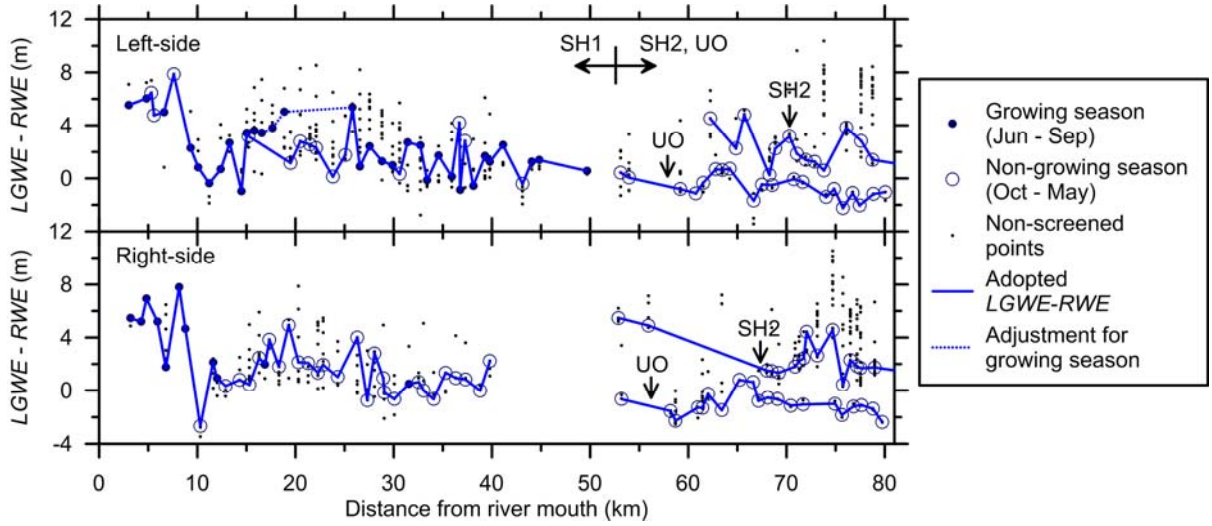

Figure 8. *LGWE-RWE* differentials predicted in both growing season (June – September) and non-growing season (October – May) along SH and UO rivers. The data gap from 40-60 km corresponds to a lack of levees (natural channel).

GROUNDWATER ELEVATION IN LEVEES ON EARTHQUAKE DATE

*LGWE*s on the earthquake dates are computed as the sum of *RWE*s shown in Figure 7 and the differentials (*LGWE-RWE*) shown in Figure 8 [non-growing season differentials were used for the 2004 earthquake (October); growing season differentials were used for the 2007 earthquake (July)]. Levee base elevations (i.e., *LBE*s) are taken at the fill-native soil contact beneath the levee crest, as indicated from boreholes and cross sections (Figure 6). We then compute the differential $D_W = LGWE - LBE$, which is shown in Figure 9 for SH1, SH2 and UO. Note that D_W has a cap of 5 m, which is the average levee height in the study region (*LGWE* cannot be higher than the levee crest). This cap is applied near the river mouth.

*LBE*s are generally lower than *LGWE*s (positive D_W) at river mouth distances less than 30 km (indicating that levee fill in this region may be saturated over some depths), and are generally higher (negative D_W) at greater river distances. The 2004 earthquake occurred two days after a flood event, so D_W values were high, particularly in downstream areas. For the 2007 earthquake, left-side levees at river mouth distances of 15-25 km have elevated *LGWE*s due to land-side irrigation, which produces relatively high D_W values. Upstream areas have similar D_W values (generally negative) for both events.

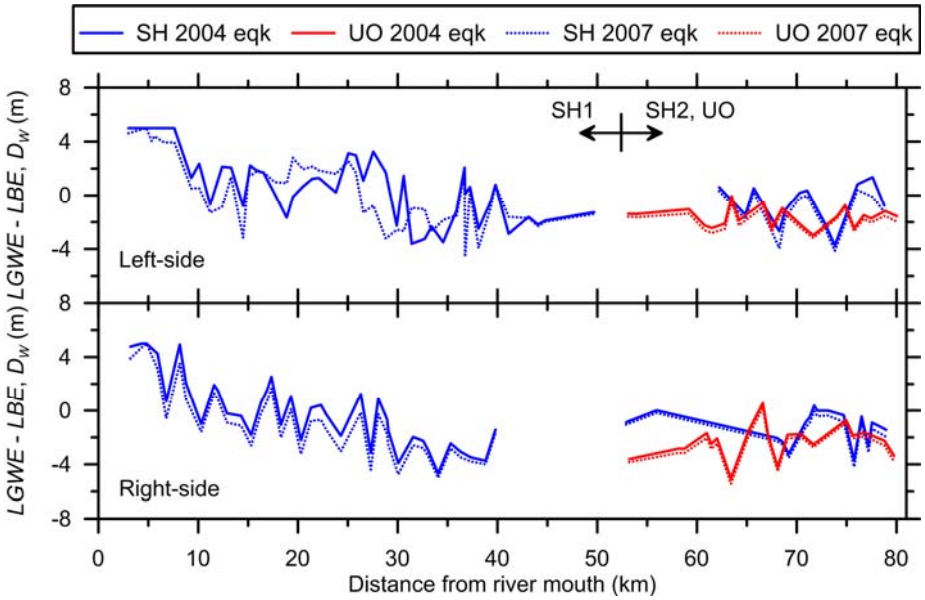

Figure 9. Profiles of differential D_W between levee groundwater elevation and levee base elevation on dates of 2004 and 2007 earthquakes.

GEOMORPHIC CONDITION AND LEVEE SHAPE

After searching many alternate sources for geologic and geomorphic data, we selected the 1:25,000 geomorphic maps prepared by the Geospatial Information Authority of Japan (GSI, 1977). These maps are made for flood control use in the vicinity of rivers, and show relatively precise boundaries of geomorphic categories (denoted G_N). Categories in these maps along the levees include mountain, terrace, alluvial fan, natural levee, alluvial plain, old river highland, old river channel, and back marsh. These geomorphic categories correlate with hydrologic conditions, and we adopt a grouping strategy proposed by Wakamatsu and Matsuoka (2011) and used by MLIT (2012) for liquefaction applications: (1) mountain and gravelly terrace, typically having deep groundwater, (i.e., groundwater depth > 3 m below ground surface); (2) alluvial fan, natural levees, alluvial plain, and old river highland, typically having shallow groundwater, (depth < 3 m); and (3) old river channel and back marsh, typically having very shallow groundwater, (depth < 1 m). The numbers of 50 m segments for each group are 264, 2485, and 312 for G_N = 1, 2, and 3, respectively.

We quantify levee shape as shape factor (S_F), computed as average levee height over average levee width. The average levee height is the mean of the left- and right-side heights from crest to toe, and the average levee width is the mean of the crest and levee base widths, including berms. These dimensions are evaluated from 157 cross sections (similar to Figure 6) and intermediate locations are spatially interpolated. The range of S_F is 0.2-0.3 for

downstream levees (relatively short and broad) and 0.25-0.35 for upstream levees (relatively slender).

EMPIRICAL ANALYSIS OF LEVEE FRAGILITY

METHODOLOGIES FOR CONSTRUCTING FRAGILITY FUNCTIONS

Methodologies for constructing fragility functions have been presented by Porter et al. (2007) and Baker (2014). An underlying assumption in those studies is that the functional form for a cumulative distribution function (CDF) (e.g., normal or log-normal) can be fit to data expressing probabilities of damage for various levels of seismic demand. The use of a CDF has the advantages of operating between the required probability range of zero to one, capturing commonly encountered data distributions, and being described by physically meaningful parameters (typically a mean and standard deviation). For example, if a log-normal CDF with mean (μ) and standard deviation (β) is fit to data on the probability of exceeding a damage level (*dl*) conditional on intensity measure *IM*, the fragility function can be defined as follows:

$$P\left(DL > dl \mid IM = im\right) = \Phi\left(\frac{\ln im - \mu}{\beta}\right) \tag{6}$$

where Φ represents the standard normal CDF with mean 0 and standard deviation 1.

Porter et al. (2007) present methodologies for computing losses in a performance-based earthquake engineering (PBEE) framework given variable levels of data quality and availability (Methods A to E, and U). Method B describes a situation in which the peak engineering demand parameters (*EDP*s, e.g., interstory drift ratios) or intensity measures (*IM*s) to which specimens were subjected are known and there is knowledge about which specimens exceeded a damage state. Method B corresponds to the situation with the subject levees, since we know where damage occurred and the associated peak levels of ground shaking have been estimated for each segment. A common characteristic of Method B is that the data does not extend to sufficiently extreme demands that the *EDP* for high failure probabilities can be empirically defined.

Baker (2014) describes methods for defining fragility functions for data conditions analogous to those associated with Method B of Porter et al. (2007). Baker considered an *EDP*|*IM* relationship, with the *EDP* being collapse and *IM* being first-mode spectral acceleration. The "data" supporting the fragility functions were derived from structural

simulations that were performed for scenario events (conditional spectra), and only certain fractions of the motions induced collapse even for large demands. Hence, the *IM*s required for high failure probabilities were often unknown (similar to the problem with Method B).

To identify the parameters describing fragility functions (μ and β in Eqn. 6), Porter et al. (2007) transform observed probabilities to their corresponding values of the standard normal variate ε (i.e., the ratio in parenthesis on the right side of Eqn. 6) using the Φ^{-1} operator, perform a least-squares linear fit of *EDP*-ε data points, and compute the moments β and μ from the slope and intercept of the fit line. Baker (2014) uses the maximized likelihood estimation (MLE) method for CDF fitting. Both approaches effectively fit the available data and extrapolate into the parameter space lacking data (i.e., for high failure probabilities). We select the MLE method since it is applicable to any functional form and minimizes the dispersion of residuals for our data set (details in Stewart et al., 2013).

PROBABILITY OF DAMAGE CONDITIONAL ON INTENSITY MEASURES ONLY

The most basic fragility function describes the probability of experiencing damage at any level [i.e., P($DL > 0$)] conditioned only on a ground motion *IM* (we have considered *PGA* and *PGV*). We denote this approach as Model 1. Probabilities of exceeding higher damage levels are addressed later.

Data on levee performance is segregated by *IM* level by organizing the data into discrete bins. The probability of levee damage for a bin j with median im_j can be calculated as follows:

$$P_j\left(DL > 0 \mid IM = im_j\right) = \frac{ND_j}{N_j} \tag{7}$$

where ND_j is the number of damaged segments and N_j is the number of total segments in bin j. Figure 10 shows distributions of damage probabilities for the *IM*s of *PGA* and *PGV*. The plot shows both damage probabilities and ND_j for each bin, which are directly related because the bins are of equal size in terms of numbers of samples, which in turn requires unequal bin width. Bin size can be related to the square-root of the total number of data points (M) as follows:

$$N_{bin} = \frac{\sqrt{M}}{4} \tag{8}$$

The use of four in the denominator is a modification of the recommendations of Porter et al. (2007), which had one in the denominator. The modification is motivated by the small number of observations for high *IM* and the need to reduce the data count requirements for those bins. Our dataset has M = 6636 levee segments, which results in N_{bin} = 20, and N_j = 6636/20 = 332 segments per bin. An advantage to this approach is that equal weight is given to each bin in the maximum likelihood estimation of the CDF moments. The fragility generally monotonically increases with *PGA* from 0.14g to 1.0g and with *PGV* from 14 cm/s to 80 cm/s. No damage occurs below approximately 0.14g or 14 cm/s and the damage probabilities reach as high as approximately 0.5 for large *IM*.

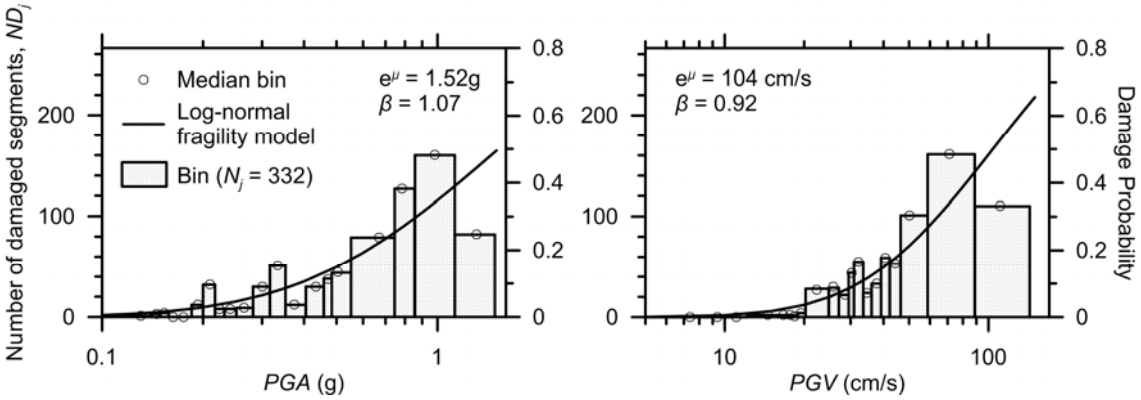

Figure 10. Probability of damage at any level conditional on intensity measures *PGA* and *PGV*. Results expressed using number of damaged segments in bins of unequal width (left) and probabilities (right). Log-normal CDF fit to data using MLE.

Figure 10 shows the fit of the log-normal CDF to the data along with the identified μ and β values. Lower values of dispersion (β) indicate increased predictive power of the *IM*. In our case, *PGV* produces modestly lower dispersion (0.92) than does *PGA* (1.07); accordingly, we utilize *PGV* as the *IM* in subsequent analysis. The dispersions shown in Figure 10 are high compared to those found in other earthquake engineering applications (e.g., values of 0.4-0.5 for many structural applications, e.g., Aslani and Miranda, 2005; Pagni and Lowes, 2006). We suspect that our relatively high β occurs because of uncertainties associated with analysis of empirical field performance data (prior studies are either analytical or use data from laboratory-scale testing); in particular, the estimation of *IM*s (not measured on-site) and the lack of detailed, section-specific, information on levee characteristics.

DAMAGE PROBABILITY CONDITIONAL ON *PGV* AND SECONDARY PARAMETERS

In this section, we evaluate *PGV*-dependent levee fragilities conditioned on surface geology of foundation soils (G_N), ground water elevation relative to the levee base (D_W), or

levee shape factor (S_F). We refer to these models collectively as Model 2. Variables G_N, D_W, and S_F are referred to as secondary parameters. The fragility computed here is the probability of damage at any level [i.e., P($DL > 0$)]; fragilities related to higher damage levels are addressed in the next section.

We considered developing a multi-parameter model using *PGV* with the secondary parameters, but instead chose to evaluate the parameters one at a time to see if they have predictive power for levee fragility. This is done by evaluating *PGV*-dependent levee fragility for selected ranges of the secondary parameters. When the data are conditioned according to these secondary parameters, there is a loss of resolution on two levels: (1) the number of *PGV*-bins is reduced per Eqn. (8), which can affect the regression of a fragility relation, particularly at high *PGV*s; (2) the number of data points per bin is reduced, decreasing the levels of confidence in the computed bin probabilities. While it is tempting to solve the second problem by using fewer bins (increasing the number of data points per bin), the first problem is then exacerbated. After some trial and error, we elected to maintain the binning criteria in Eqn. (8) for use in Model 2 regressions and not change the value '4' in the denominator.

We seek to identify which of the secondary variables affect levee fragility by investigating conditions for which the differences between Model 2 and Model 1 are statistically significant. We define μ_{r1} and μ_{r2} as the means of residuals of Model 1 and Model 2 data points, respectively, relative to Model 1 predictions. If the residuals are plotted against *PGV*, the resulting slopes are b_{r1} and b_{r2} (using Model 1 and 2 data points, respectively). The distinction between Model 1 and Model 2 is then judged on the basis of *t*-tests with two null hypotheses:

1. H_{01}: hypothesis is that $\mu_{r1} - \mu_{r2} = 0$ (the two means are identical),
2. H_{02}: hypothesis is that $b_{r1} - b_{r2} = 0$ (the two slopes are identical).

Note that μ_{r1} and b_{r1} are approximately zero since Model 1 is regressed from Model 1 data points.

Rejection of the null hypothesis is expressed as a *p*-value indicating the level of significance. The *p*-value is the probability of exceeding the *t* variate in the *t*-distribution with *df* degrees of freedom; details of this calculation are provided in the Electronic Supplement. A *p*-value of 10% or less is often used to indicate that the null hypothesis can be rejected with

confidence, although this 10% limit is arbitrary. The data for Models 1 and 2 can be considered as distinct if either one or both null hypotheses are rejected. The *p*-values in Table A.1 (electronic supplement) show that among the 23 investigated conditions, one G_N condition (i.e., $G_N = 1$) and one D_W conditions (i.e., $D_W < -2.5$ m) result in $p < 0.10$. The D_W conditions indicating shallow ground water levels (i.e., $D_W > d_w$) are not strictly distinct from Model 1. Moreover, shape factor S_F was not found to be a significant secondary parameter. These results lead us to further examine G_N and D_W fragilities and to abandon S_F.

Figure 11 shows fragility curves conditioned on G_N. The most common category comprising 81% of levee segments is G_N 2 (various alluvial sediments), which has fragilities nearly identical to Model 1. Fragilities for G_N 1 (mountain and terrace) are relatively low. The curve for G_N 3 (old river channel and back marsh) is relatively steep due to reduced fragility for $PGV \leq 30$ cm/s, but the data is sufficiently sparse that its distinction from Model 1 is not justified. Accordingly, we conclude that G_N 2 and 3 are similar to Model 1 but G_N 1 is distinct.

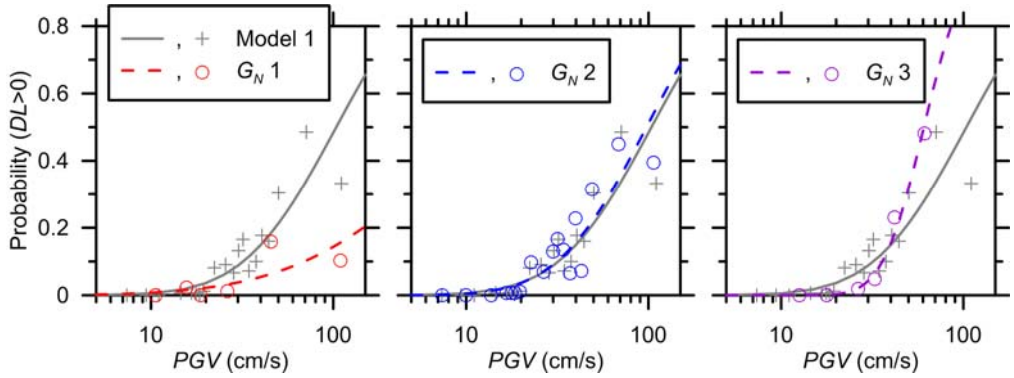

Figure 11. Model 2 fragility functions conditional on G_N groups.

Figure 12 shows fragility curves conditioned on D_W, with the upper set of plots corresponding to relative shallow groundwater ($D_W > d_w$) and the lower set corresponding to deep groundwater ($D_W < d_w$). We expect higher fragilities for the shallow groundwater case due to greater liquefaction susceptibility. The fragilities are nominally similar for $PGV < 30$ cm/s; these ground motion levels appear to be too low to induce significant liquefaction. For stronger shaking, shallow groundwater conditions ($D_W > -1$ m and $D_W > 0$) give rise to fragilities greater than Model 1, whereas results for deep groundwater conditions are more mixed. The greatest differences are for $D_W > -1$ m and $D_W < -1$ m, which fall consistently above and below Model 1 fragilities for $PGV > 30$ cm/s. While the fits for these cases are not statistically distinct relative to Model 1 (as shown in Electronic Supplement), the shallow and

deep groundwater models are distinct from each other at 93% confidence (p-value = 0.07). using the slope-based t-test (i.e., H_{02} hypothesis). We adopt D_W as a Model 2 conditioning variable because: (1) it makes physical sense; (2) the fragility curves are indeed divergent and constrained by data for the important range of $PGV > 30$ cm/s; and (3) this conditioning has greater statistical significance in subsequent analysis involving higher damage level thresholds.

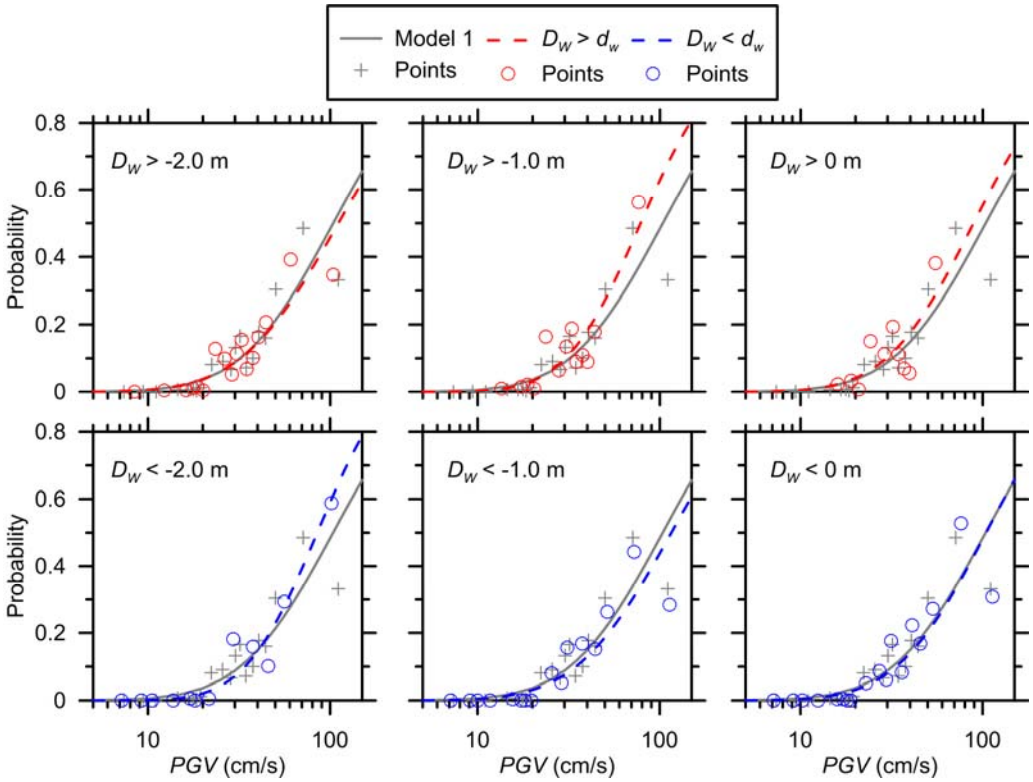

Figure 12. Model 2 fragility functions conditional on D_W groups.

Of the 2624 segments that have D_W > -1.0 m, 1605 (61%) have a fully saturated foundation ($D_W > 0$ m) and the median value of D_W is 0.4 m. Hence for practical purposes, the D_W > -1.0 m bin represents conditions with a reasonable probability of liquefaction susceptibility (provided that the soils are granular). For the deep ground water case of D_W < -1.0 m, the median D_W is -2.1 m for a large data population of 4012 segments.

Table 2 indicates moments of log-normal CDFs (i.e., mean μ and standard deviation β), standard deviation of residual (σ), and valid PGV range for versions of Model 2 based on G_N 1 and the recommended D_W limits. The corresponding values for Model 1 are also shown for reference purposes along with similarly derived results using the IM of PGA. The Model 2 β value for D_W > -1.0 m is smaller than that from Model 1, indicating improved resolution of the fragility function. There is practically no change in β for the deep groundwater case.

Table 2. Moments of log-normal CDFs (μ and β) for *PGV*- and *PGA*-based fragility curves standard deviation of residuals (σ), and valid *IM* ranges.

Model	*IM*	Condition	μ	e^{μ}	β	σ	Range
Model 1		*PGV*	4.64	104 cm/s	0.92	0.07	7 ~ 111 cm/s
		PGA	0.42	1.52g	1.07	0.07	0.13 ~ 1.31g
Model 2	*PGV*	G_N 1	6.42	611 cm/s	1.70	0.05	10 ~ 110 cm/s
		D_W < -1.0 m	4.75	116 cm/s	0.94	0.07	7 ~ 114 cm/s
		D_W > -1.0 m	4.36	78 cm/s	0.74	0.06	13 ~ 77 cm/s
	PGA	G_N 1	2.59	13.4g	2.02	0.03	0.14 ~ 1.29g
		D_W < -1.0 m	0.41	1.51g	0.92	0.08	0.13 ~ 1.33g
		D_W > -1.0 m	0.26	1.30g	1.12	0.07	0.14 ~ 1.07g

PROBABILITIES OF EXCEEDING SPECIFIC DAMAGE LEVELS

We examine the probabilities of exceeding various damage levels conditional on some damage having occurred [i.e., P($DL > dl \mid DL > 0$)]. We examine the possible dependence of these failure probabilities on geomorphology (G_N) and groundwater level (D_W). We look for the possibility of *PGV*-dependent conditional damage probabilities, and when no such dependence is found, we provide *PGV*-independent mean probabilities (P_m). The *PGV*-dependent probabilities are described using a log-normal CDF (as above).

Figure 13 shows the conditional fragility data (damage thresholds of $DL > 1$, 2, and 3) for the full data set (no conditioning on secondary parameters) and binned according to the secondary parameters identified in the previous section. The full data set indicates *PGV*-independent fragility for all damage levels. For G_N 1, $DL > 1$ shows *PGV*-independent fragility, $DL > 2$ has finite probability only at high *PGV* (> 50 cm/s), and no instances of $DL > 3$ were reported. Cases with deep groundwater (D_W < -1 m; selected on basis of low *p*-values as indicated in Table A.1) have *PGV*-dependent fragilities for $DL > 1$, 2 and 3. Deep groundwater conditions are less susceptible to liquefaction, so the principal damage mechanism for levees is expected to be slope deformation, which has been correlated to various intensity measures including *PGA* and *PGV* in past work (Saygili and Rathje, 2008). We find *PGV*-independent fragilities for shallow groundwater (D_W > -1 m). Because levee damage for these shallow groundwater cases is largely caused by liquefaction, the data indicate that the level of damage is not *PGV*-dependent once damage is triggered. Comparing the conditional fragilities for the deep and shallow ground water cases indicates increased

probability of each higher damage threshold for shallow as compared to deep ground water. This shows that shallow ground water not only increases the probability of damage, but also the severity of damage.

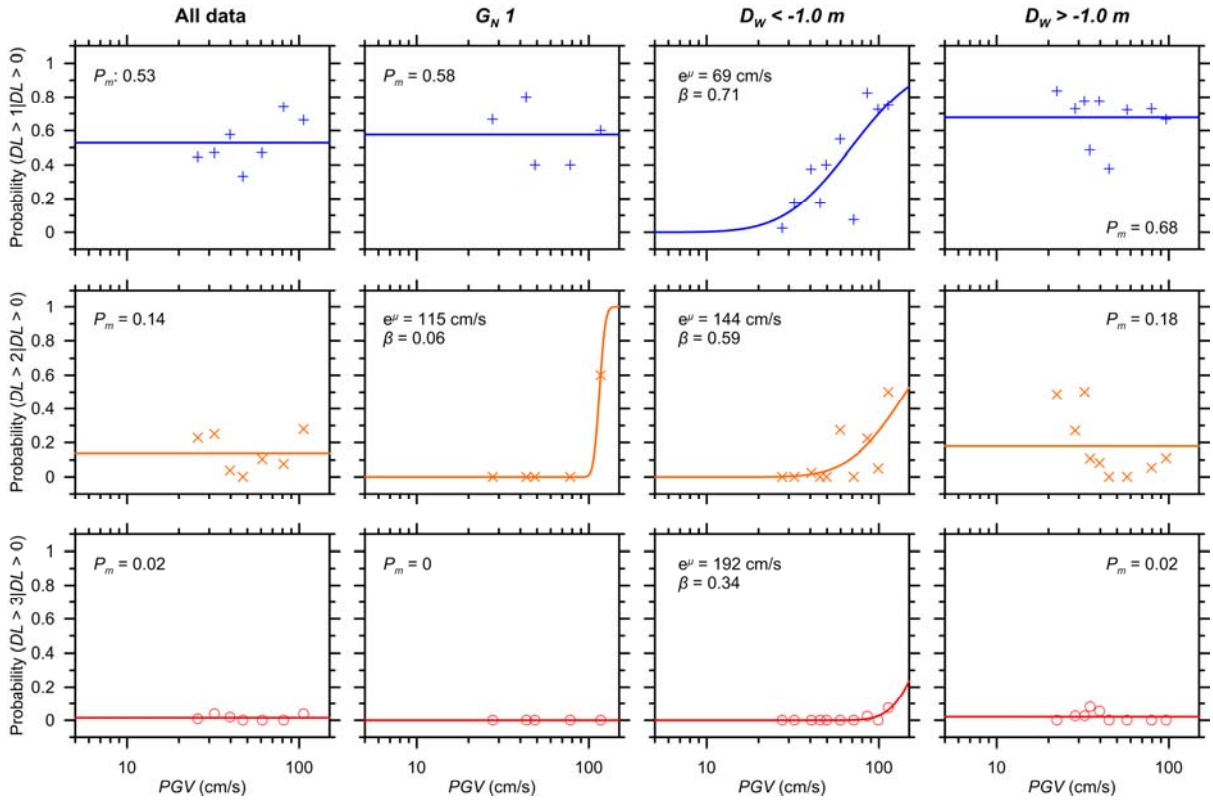

Figure 13. Probability of exceeding damage levels above one for the full data set and sets with geomorphic (G_N) and groundwater level (D_W) conditions. Moments of log-normal CDF (mean and standard deviation; μ and β) are indicated for *PGV*-dependent cases otherwise mean probabilities (P_m) are indicated.

Using the total probability theorem (e.g., Ang and Tang, 2007), these conditional damage fragilities can be combined with the fragilities from prior sections (for damage at any level) to develop a fragility function for any desired damage level as follows:

$$P(DL > dl \mid PGV, SP) = P(DL > 0 \mid PGV, SP) \times P(DL > dl \mid DL > 0, PGV, SP) \quad (9)$$

where *SP* represents secondary parameters used for Model 2 conditions. For Model 1, *SP* is disregarded. For an example of Model 2 probability, consider *PGV* = 40 cm/s and shallow ground water condition (i.e., D_W > -1.0 m). The probability of damage is 0.18 and the P_m for *DL* > 2 is 0.18. The product results in a probability of 0.03 for *DL* > 2.

SUMMARY AND CONCLUSIONS

We have developed empirical fragility functions for the seismic performance of flood control levees subjected to strong ground motion from two **M** 6.6 shallow crustal earthquakes

in Japan. The embankment and foundation soil conditions are such that liquefaction susceptibility exists for a subset of the levees, but additional ground failure mechanisms including seismic slope instability and seismic compression contribute to observed levee deformations.

The data set is largely derived from various agencies under the Ministry of Land, Infrastructure, Transportation and Tourism (MLIT) in Japan. The compiled dataset includes damage levels (*DL*) and supporting damage descriptions; estimated ground motion intensity measures (*PGA* and *PGV*); evaluations of hydrological conditions, which produce estimates of the vertical distance between the groundwater level in levees and the elevation of the levee base beneath the crest (D_W); a geomorphic description of the foundation soil conditions (G_N); and a quantification of levee shape as approximate height/width ratio (S_F). We developed these parameters for 50 m (in length) levee segments over 166 km of levees along the Shinano River system.

Fragility functions express the probability of exceeding a damage level (*DL*) conditioned on intensity measures (*IM*s) alone (i.e., Model 1) and *IM*s in combination with other parameters (Model 2). We find that *PGV* correlates more strongly to damage occurrence than *PGA*. Model 1 results indicate no damage below approximately 14 cm/s and a monotonic increase of failure probability to 0.5 at 80 cm/s. Statistical tests indicate that secondary parameters significantly impacting damage probabilities include G_N and D_W. In particular, the relatively competent soil conditions associated with G_N 1 (mountain and terrace) have lower damage probabilities than the general data population. Moreover, shallow ground water conditions (D_W > -1 m) produce higher damage probabilities, by approximately 40 percent, than those for deep ground water conditions in the moderate to high *PGV* range.

We also compile probabilities of exceeding various damage levels conditioned on some damage having occurred. These conditional fragilities are generally *PGV*-dependent for non-liquefaction susceptible sites (typically deep ground water conditions) and *PGV*-independent for liquefaction susceptible sites (typically shallow ground water conditions). Fragilities decrease with increasing damage levels and increase for shallow ground water conditions.

The levee fragility models developed in this work are strictly applicable for the conditions along the Shinano River in Japan for $PGV \leq 140$ cm/s and **M** 6.6 earthquakes. Their applicability to other regions, such as those present along flood control levees in California's Central Valley, are dependent on the similarity of the seismological,

geotechnical, and hydrological conditions (Kwak et al., 2014). Where this compatibility can be demonstrated, the proposed fragility relations are useful for preliminary levee risk assessments in which detailed geotechnical data are unavailable. We note that these relations are incomplete, however, in the sense that an assessment of levee system risk also requires knowledge of the spatial correlations of levee damage, which is not part of the present work. That issue, and the quantification of levee fragility when analyzed using site-specific geotechnical procedures, will be addressed in subsequent work. The fragility functions presented in this paper are not applicable to levees that constantly impound water, such as those in the Sacramento – San Joaquin Delta, which we anticipate to be more susceptible to earthquake-induced damage due to the predominance of shallow saturated sediments.

ACKNOWLEDGEMENTS

This work was supported by California Department of Water and Resource (CDWR) under contract number 4600008849. This support is gratefully acknowledged. Any opinions, findings, and conclusions or recommendations expressed in this material are those of the authors and do not necessarily reflect those of the CDWR. We also acknowledge data providers, i.e., Ministry of Land, Infrastructure, Transportation and Tourism (MLIT), Shinano River Work Office (SWO), Niigata Prefectural Office (NPO), National Research Institute for Earth Science and Disaster Prevention (NIED), Geological Survey of Japan (GSJ), East Japan Railway Company, NEXCO East Japan, and Kashiwazaki City. We also thank our collaborators, Raymond B. Seed and Juan M. Pestana at the University of California at Berkeley (UCB), Ariya Balakrishnan at CDWR, Leslie F. Harder, Jr. at HDR Inc., and Vlad G. Perlea at U.S. Army Corps of Engineers (USACE) for their valuable comments and suggestions.

REFERENCES

Ang, A. H-S., and Tang, W. H., 2007. *Probability concepts in engineering: emphasis on applications to Civil and Environmental Engineering*, *2nd Edition*, Wiley, New York, 420 pp.

Apel, H., Thieken, A. H., Merz, B., and Blöschl, G., 2004. Flood risk assessment and associated uncertainty, *Nat. Hazards Earth Syst. Sci.* **4**(2), 295–308.

Asano, K., and Iwata, T., 2009. Source rupture process of the 2004 Chuetsu, Mid-Niigata Prefecture, Japan, Earthquake inferred from waveform inversion with dense strong-motion data, *Bull. Seism. Soc. Am.* **99**(1), 123–140.

Aslani, H., and Miranda, E., 2005. Fragility assessment of slab-column connections in existing non-ductile reinforced concrete buildings, *J. Eqk. Eng.* **9**(6), 777–804.

Baker, J. W., 2014. Efficient analytical fragility function fitting using dynamic structural analysis, *Earthquake Spectra*, in-press.

Boore, D. M., Stewart, J. P., Seyhan, E., and Atkinson, G. M., 2014. NGA-West 2 equations for predicting PGA, PGV, and 5%-damped PSA for shallow crustal earthquakes, *Earthquake Spectra*, in-press.

Food and Agriculture Organization of the United Nations (FAO), 2004. *International year of rice 2004*. (last accessed from http://www.fao.org/rice2004/index_en.htm at February 2014)

Geospatial Information Authority of Japan (GSI), 1977. *Geomorphological map for flood control use* (in Japanese). (last accessed from http://www1.gsi.go.jp/geowww/lcmfc/lcmfc.html at February 2014)

Kwak, D. Y., Brandenberg, S. J., Mikami, A., Balakrishnan, A., and Stewart, J. P., 2014. Applicability of levee fragility functions developed from Japanese data to California's Central Valley, *2014 Annual Meeting and Conf. on U.S. Soc. Dams*, San Francisco, CA.

Kwak, D. Y., Mikami, A., Brandenberg, S. J., and Stewart, J. P., 2012. Ground motion estimation for evaluation of levee performance in past earthquakes, *9th Int. Conf. Urban Eqk. Eng./4th Asia Conf. Eqk. Eng.*, Tokyo Institute of Technology, Tokyo, Japan.

Miller, E. A., and Roycroft, G. A., 2004. Seismic performance and deformation of levees: four case studies, *J. Geotech. & Geoenvir. Eng.* **130**(4), 344–354.

Ministry of Land, Infrastructure, Transport and Tourism (MLIT), 2012. *Inspection manual of seismic levee performance regarding Level 2 earthquake* (in Japanese), MLIT.

Miyake, H., Koketsu, K., Hikima, K., Shinohara, M., and Kanazawa, T., 2010. Source fault of the 2007 Chuetsu-oki, Japan, Earthquake, *Bull. Seism. Soc. Am.* **100**(1), 384–391.

Oppenheim, A. V., and Schafer, R. W., 2010. *Discrete-time signal processing, 3rd Edition*, Prentice Hall, 1120 pp.

OYO, 2008. *Investigation of liquefaction in the Shinano River* (in Japanese), OYO, Co., Ltd.

Pagni, C. A., and Lowes, L. N., 2006. Fragility functions for older reinforced concrete beam-column joints, *Earthquake Spectra* **22**(1), 215–238.

Porter, K., Kennedy, R., and Bachman, R., 2007. Creating fragility functions for Performance-Based Earthquake Engineering, *Earthquake Spectra* **23**(2), 471–489.

Rosidi, D., 2007. Seismic risk assessment of levees, *Civil Engineering Dimension* **9**(2), 57–63.

Sasaki, Y., 2009. River dike failures during the 1993 Kushiro-oki Earthquake and the 2003 Tokachi-oki Earthquake, *Earthquake Geotechnical Case Histories for Performance-Based Design*, T. Kokusho (editor), 131–157.

Sawada, S., Suetomi, I., Fukushima, Y., and Goto, H., 2008. Characteristics and distribution of strong ground motion during the 2004 Niigata-ken Chuetsu and 2007 Niigata-ken Chuetsu-oki Earthquake in Japan, *Proc. 14th World Conf. Eqk. Eng.*, Oct 12-17, 2008, Beijing, China.

Saygili, G., and Rathje, E. M., 2008. Empirical predictive models for earthquake-induced sliding displacements of slopes, *J. Geotech. & Geoenvir. Eng.* **134**(6), 790–803.

Shinano River Work Office (SWO), 2007. *Report of damage survey and estimation of the Shinano River by 2007 Niigata-ken Chuetsu-oki Earthquake* (in Japanese).

Shinano River Work Office (SWO), 2008. *Log of the 2004 Niigata-ken Chuetsu Earthquake by Shinano River Work Office* (in Japanese).

Stewart, J. P., Kwak, D. Y., Brandenberg, S. J., and Mikami, A., 2013. *Characterization of seismic fragility of levees using field performance data*, *Project Report for California Department of Water Resources*, UCLA, 142 pp.

Sugita, H., and Tamura, K., 2008. Development of seismic design criteria for river facilities against large earthquakes, *Proc. 14th World Conf. Eqk. Eng.*, Oct 12-17, 2008, Beijing, China.

Salah-Mars, S., Rajendram, A., Kulkarni, R., McCann, M. W. Jr., Logeswaran, S., Thangalingam, K., Svetich, R., and Bagheban, S., 2008. Seismic vulnerability of the Sacramento-San Joaquin Delta levees, *Geotech. Eng. & Soil Dyn. IV*, May 18-22, 2008, Sacramento, CA, 1–10.

Foster, J. L., et al., 2009. *Performance evaluation of the New Orleans and Southeast Louisiana Hurricane Protection System*, *vol. VIII–Engineering and operational risk and reliability analysis*, *Final Report of the Interagency Performance Evaluation Task Force*, U.S. Army Corps of Engineers, Washington, DC.

U.S. Army Corps of Engineers (USACE), 2011. *Guidelines for seismic stability evaluation of levees*, USACE Sacramento District.

Vorogushyn, S., Merz, B., and Apel, H., 2009. Development of dike fragility curves for piping and micro-instability breach mechanisms, *Nat. Hazards Earth Syst. Sci.* **9**(4), 1383–1401.

Wakamatsu, K., and Matsuoka, M., 2011. Developing a 7.5-sec site-condition map for Japan based on geomorphologic classification, *Eqk. Res. Eng. Str. VIII*, 101–112.

Yamazaki, F., Motomura, H., and Hamada, T., 2000. Damage assessment of expressway networks in Japan based on seismic monitoring, *Proc. 12th World Conf. Eqk. Eng.,* Auckland, New Zealand.